

A NEW SATELLITE IMAGE FUSION METHOD BASED ON DISTRIBUTED COMPRESSED SENSING

Fulin Li, Shaohua Hong and Lin Wang

Xiamen University
Department of Communication Engineering
Fujian, China

ABSTRACT

In this paper, we propose a method for fusion of low-resolution multispectral (LRM) image and high-resolution panchromatic (HRP) image to obtain high-resolution multispectral (HRM) image based on distributed compressed sensing (DCS). In the proposed method, HRP image is firstly used to obtain approximation and detail dictionary. Then, joint-sparsity-model-1 (JSM-1) is applied directly to both LRM bands and HRM bands. Each band in LRM image is decomposed into common component and innovation component which can be sparsely represented over the approximation dictionary. Based on Orthogonal Matching Pursuit (OMP) algorithm, the sparse coefficients are calculated from JSM-1 of the LRM image. Lastly, each band in HRM image is modeled as the fusion of the corresponding LRM band and detail band over the detail dictionary. Two datasets are used in the experiments to validate the proposed method and the results show that the proposed method has better performance than the traditional methods.

Index Terms— Distributed compressed sensing, high-resolution panchromatic image, joint sparsity model, low-resolution multispectral image, satellite image fusion.

1. INTRODUCTION

Satellite imaging is a vital topic to obtain high-resolution images of observed target. Usually, satellite imaging sensors include multispectral (MS) sensors and panchromatic (PAN) sensors. Due to constraints of received energy and physics of sensors, MS image detected by MS sensors is of high spectral resolution and low spatial resolution, named as LRM image, while PAN image detected by PAN sensors is of low spectral resolution and high spatial resolution, named as HRP image. Fusion of satellite images is used to obtain a high resolution multispectral (HRM) image. This process is also called as pan-sharpening in some occasions. Satellite image fusion matters very much in practical applications, which provides rich surface information for reference [1].

In recent years, many methods have been proposed for

satellite image fusion, which can be divided into four categories including component substitution methods, multi-resolution analysis (MRA) methods, hybrid methods, and restoration-based methods [2]. Typical component substitution methods are Intensity-Hue-Saturation (IHS) method [3], Gram-Schmidt (GS) method [4] and BDSD method [5]. MRA methods are usually based on transform domain, which mainly include methods of wavelet transform [6] and curvelet transform [7]. Hybrid methods are the combination of component substitution and MRA method [8]. An IHS and curvelet transform combined method is proposed in [9], which utilizes the portraits of both methods. Restoration-based methods try to find a correlation model among LRM, HRP and HRM image. Fusion approaches based on compressed sensing are typical methods in restoration-based methods. In [10], LRM image is modeled as a degraded version of HRM image and HRP image as a linear combination of HRM bands. Then, it establishes two models for fusion and compressed sensing is utilized to solve the models. In general, component substitution methods tend to utilize the spatial resolution of HRP image but cannot keep the spectral characteristics of original LRM image. MRA methods are featured by preserving the spectral features of LRM image while losing detail information in the spatial domain for the fused HRM image. Compressed-sensing based fusion methods are capable of making better use of the high spectral resolution in LRM image and high spatial resolution in HRP image. However, it does not consider the inter-signal correlation in LRM and HRM bands. To exploit the inter-signal correlation, methods based on distributed compressed sensing (DCS) [11] are proposed in [12] and [13] and have been demonstrated to show better performance. DCS constructs joint sparsity model (JSM) among correlated signals, which can extract features of such signals. However, the framework in [12] and [13] establishes dictionary in the transform domain, which may not make full use of correlation among image signals. To solve this problem, a new DCS-based fusion method is proposed in this paper, where JSM-1 is applied directly to both LRM and HRM bands to exploit the inter-signal correlation in LRM and HRM bands.

The remainder of this paper is organized as follows. In Section 2, we describe the proposed method in detail. Experiments and discussions are followed in Section 3. Finally, conclusion is stated in Section 4.

2. PROPOSED FUSION METHOD

2.1. Distributed Compressed Sensing (DCS)

Distributed compressed sensing [11] extends the compressed sensing theory to multiple signals that are correlated with each other. With compressed sensing theory, a signal can be reconstructed by

$$\mathbf{x}^{est} = \Phi\alpha, \alpha = \min_{\alpha} \|\alpha\|_0, \text{ s.t. } \|\mathbf{y} - \mathbf{M}\Phi\alpha\|_2^2 \leq \varepsilon \quad (1)$$

where ℓ_0 norm represents the number of non-zero elements and ε is the reconstruction error, $\mathbf{y} \in \mathbb{R}^{m \times 1}$ is the observation vector of $\mathbf{x} \in \mathbb{R}^{n \times 1}$, $\mathbf{M} \in \mathbb{R}^{m \times n}$ is the measurement matrix, $\Phi \in \mathbb{R}^{n \times N}$ is the dictionary, and $\alpha \in \mathbb{R}^{N \times 1}$ is the sparse coefficient. The problem mentioned above is NP-hard factually, which resultantly leads to development of many sub-optimal algorithms such as basis pursuit algorithm and orthogonal matching pursuit (OMP) algorithm [14].

There have been three joint sparsity models (JSM) to exploit inter-signal correlation [11], called as JSM-1, JSM-2, and JSM-3. In JSM-1, each signal is divided into common component and innovation component. In our proposed method, JSM-1 is applied in image fusion. Supposing that $\mathbf{X} = [\mathbf{x}_1^T, \mathbf{x}_2^T, \dots, \mathbf{x}_J^T]^T \in \mathbb{R}^{Jn \times 1}$ is a correlated signal ensemble, according to JSM-1, signals in \mathbf{X} can be written as

$$\begin{aligned} \mathbf{x}_1 &= \mathbf{z}_c + \mathbf{z}_1 \\ \mathbf{x}_2 &= \mathbf{z}_c + \mathbf{z}_2 \\ &\dots \\ \mathbf{x}_J &= \mathbf{z}_c + \mathbf{z}_J \end{aligned} \quad (2)$$

where J is the number of signals, \mathbf{z}_c is the common component, and $\mathbf{z}_1, \mathbf{z}_2, \dots, \mathbf{z}_J$ are the innovation components. Decomposing \mathbf{z}_c and \mathbf{z}_j ($j = 1, 2, \dots, J$) into linear combination of atoms in dictionaries, we have

$$\mathbf{z}_c = \Phi_c \alpha_c, \mathbf{z}_j = \Phi_s \alpha_j \quad (3)$$

where Φ_c is the dictionary for common component, Φ_s is the dictionary for innovation component, α_c and α_j are the sparse coefficients for common and innovation component. Thus, equation (2) can be expressed in matrix form as follows:

$$\mathbf{X} = \begin{bmatrix} \Phi_c & \Phi_s & 0 & \cdots & 0 \\ \Phi_c & 0 & \Phi_s & \cdots & 0 \\ \vdots & \vdots & \vdots & \ddots & \vdots \\ \Phi_c & 0 & 0 & \cdots & \Phi_s \end{bmatrix} \begin{bmatrix} \alpha_c \\ \alpha_1 \\ \vdots \\ \alpha_J \end{bmatrix} \quad (4)$$

Based on compressed sensing theory, we have

$$\mathbf{Y} = \mathbf{MX} = \mathbf{M}\Phi\alpha =$$

$$\begin{bmatrix} \mathbf{M}_1 & 0 & \cdots & 0 \\ 0 & \mathbf{M}_2 & \cdots & 0 \\ \vdots & \vdots & \ddots & \vdots \\ 0 & 0 & \cdots & \mathbf{M}_J \end{bmatrix} \begin{bmatrix} \Phi_c & \Phi_s & 0 & \cdots & 0 \\ \Phi_c & 0 & \Phi_s & \cdots & 0 \\ \vdots & \vdots & \vdots & \ddots & \vdots \\ \Phi_c & 0 & 0 & \cdots & \Phi_s \end{bmatrix} \begin{bmatrix} \alpha_c \\ \alpha_1 \\ \vdots \\ \alpha_J \end{bmatrix} \quad (5)$$

where $\mathbf{y}_j \in \mathbb{R}^{m \times 1}$, $\mathbf{Y} = [\mathbf{y}_1^T, \mathbf{y}_2^T, \dots, \mathbf{y}_J^T]^T$ is the observation matrix, $\mathbf{M}_j \in \mathbb{R}^{m \times n}$ is the measurement matrix, $j = 1, 2, \dots, J$. Consequently, the reconstruction problem comes to the following

$$\mathbf{X}^{est} = \Phi\alpha, \alpha = \min_{\alpha} \|\alpha\|_0, \text{ s.t. } \|\mathbf{Y} - \mathbf{M}\Phi\alpha\|_2^2 \leq \varepsilon \quad (6)$$

In our proposed model, \mathbf{X} denotes the up-sampled LRM image, which has the same size as HRM image,

2.2. Fusion Model Formulation

Let \mathbf{H} denote the HRM image that we desire to obtain with image fusion method and \mathbf{P} denote the HRP image. With the reasonable assumption that \mathbf{H} can be modeled as the linear combination of image patches in \mathbf{P} , we have

$$\mathbf{h}_k^i = \mathbf{D}_{HRP} \alpha_k^i, i = 1, 2, \dots, Q, k = 1, 2, \dots, B \quad (7)$$

where \mathbf{h}_k^i is the i th image patch in k th band of \mathbf{H} , \mathbf{D}_{HRP} is the dictionary obtained from \mathbf{P} , α_k^i is the corresponding sparse coefficient, Q is the number of image patches, and B is the number of bands.

For the up-sampled LRM image denoted as \mathbf{X} , each image patch in k th band can be similarly written as

$$\mathbf{x}_k^i = \mathbf{D}_{app} \alpha_k^i, i = 1, 2, \dots, Q, k = 1, 2, \dots, B \quad (8)$$

where \mathbf{D}_{app} is the low-pass version of \mathbf{D}_{HRP} and can be produced from the low-pass version \mathbf{P}_L of \mathbf{P} . In the proposed model, \mathbf{P}_L is obtained with the help of modulation transfer function (MTF) of the PAN sensor. To get the dictionary \mathbf{D}_{app} , we can simply tile \mathbf{P}_L into image patches of size $K \times K$ with $r\%$ overlap between adjacent image patches and subtract the mean from each image patch.

Without loss of generality, \mathbf{H} is constructed by adding corresponding details to \mathbf{X} [15], given by

$$\mathbf{h}_k^i = \mathbf{x}_k^i + \mathbf{d}_k^i \quad (9)$$

where \mathbf{d}_k^i is the detail patch of the i th image patch in k th band of \mathbf{H} . That is to say, \mathbf{x}_k^i is approximated as the low-pass version of \mathbf{h}_k^i in the proposed model.

Similarly, the details \mathbf{d}_k^i can be given by

$$\mathbf{d}_k^i = \mathbf{D}_{det} \alpha_k^i \quad (10)$$

where \mathbf{D}_{det} is the high-pass version of \mathbf{D}_{HRP} and can be produced from the high-pass version of \mathbf{P} from $\mathbf{P} - \mathbf{P}_L$.

Therefore, each image patch in k th band of \mathbf{H} can be obtained by

$$\mathbf{h}_k^i = \mathbf{x}_k^i + \mathbf{D}_{det}\alpha_k^i \quad (11)$$

All bands in LRM image can be seen as a signal ensemble, among which each band is correlated with the other bands. It is the same for all the bands in HRM image. According to JSM-1 model, it is easy to get the following equation

$$\begin{bmatrix} \mathbf{x}_1^i \\ \mathbf{x}_2^i \\ \vdots \\ \mathbf{x}_B^i \end{bmatrix} = \begin{bmatrix} \mathbf{D}_{app} & \mathbf{D}_{app} & \mathbf{0} & \cdots & \mathbf{0} \\ \mathbf{D}_{app} & \mathbf{0} & \mathbf{D}_{app} & \cdots & \mathbf{0} \\ \vdots & \vdots & \vdots & \ddots & \vdots \\ \mathbf{D}_{app} & \mathbf{0} & \mathbf{0} & \cdots & \mathbf{D}_{app} \end{bmatrix} \begin{bmatrix} \alpha_c^i \\ \alpha_1^i \\ \vdots \\ \alpha_B^i \end{bmatrix} \quad (12)$$

where α_c^i is the common sparse coefficient for the i th image patch and α_k^i ($k = 1, 2, \dots, B$) is the innovation coefficient for the i th image patch in k th band of \mathbf{X} . Thus, the observation matrix given in Equation (5) can be rewritten as

$$\begin{bmatrix} y_1^i \\ y_2^i \\ \vdots \\ y_B^i \end{bmatrix} = \mathbf{M} \begin{bmatrix} \mathbf{x}_1^i \\ \mathbf{x}_2^i \\ \vdots \\ \mathbf{x}_B^i \end{bmatrix} = \begin{bmatrix} \mathbf{M}_1 & \mathbf{0} & \cdots & \mathbf{0} \\ \mathbf{0} & \mathbf{M}_2 & \cdots & \mathbf{0} \\ \vdots & \vdots & \ddots & \vdots \\ \mathbf{0} & \mathbf{0} & \cdots & \mathbf{M}_B \end{bmatrix} \times \begin{bmatrix} \mathbf{D}_{app} & \mathbf{D}_{app} & \mathbf{0} & \cdots & \mathbf{0} \\ \mathbf{D}_{app} & \mathbf{0} & \mathbf{D}_{app} & \cdots & \mathbf{0} \\ \vdots & \vdots & \vdots & \ddots & \vdots \\ \mathbf{D}_{app} & \mathbf{0} & \mathbf{0} & \cdots & \mathbf{D}_{app} \end{bmatrix} \begin{bmatrix} \alpha_c^i \\ \alpha_1^i \\ \vdots \\ \alpha_B^i \end{bmatrix} \quad (13)$$

where \mathbf{y}_k^i ($k = 1, 2, \dots, B$) is the observation of \mathbf{x}_k^i , $\mathbf{M}_1 = \mathbf{M}_2 = \dots = \mathbf{M}_B$, $\mathbf{M}_k \in \mathbb{R}^{m \times n}$, $n = K \times K$.

In order to solve (13) to obtain the sparse coefficients, OMP algorithm is utilized. Once the sparse coefficients are gotten, we can construct the HRM image, given by

$$\begin{bmatrix} \mathbf{h}_1^i \\ \mathbf{h}_2^i \\ \vdots \\ \mathbf{h}_B^i \end{bmatrix} = \begin{bmatrix} \mathbf{x}_1^i \\ \mathbf{x}_2^i \\ \vdots \\ \mathbf{x}_B^i \end{bmatrix} + \begin{bmatrix} \mathbf{d}_1^i \\ \mathbf{d}_2^i \\ \vdots \\ \mathbf{d}_B^i \end{bmatrix} = \begin{bmatrix} \mathbf{x}_1^i \\ \mathbf{x}_2^i \\ \vdots \\ \mathbf{x}_B^i \end{bmatrix} + \begin{bmatrix} \mathbf{D}_{det} & \mathbf{D}_{det} & \mathbf{0} & \cdots & \mathbf{0} \\ \mathbf{D}_{det} & \mathbf{0} & \mathbf{D}_{det} & \cdots & \mathbf{0} \\ \vdots & \vdots & \vdots & \ddots & \vdots \\ \mathbf{D}_{det} & \mathbf{0} & \mathbf{0} & \cdots & \mathbf{D}_{det} \end{bmatrix} \begin{bmatrix} \alpha_c^i \\ \alpha_1^i \\ \vdots \\ \alpha_B^i \end{bmatrix} \quad (14)$$

Fig.1 shows the flowchart of our proposed method.

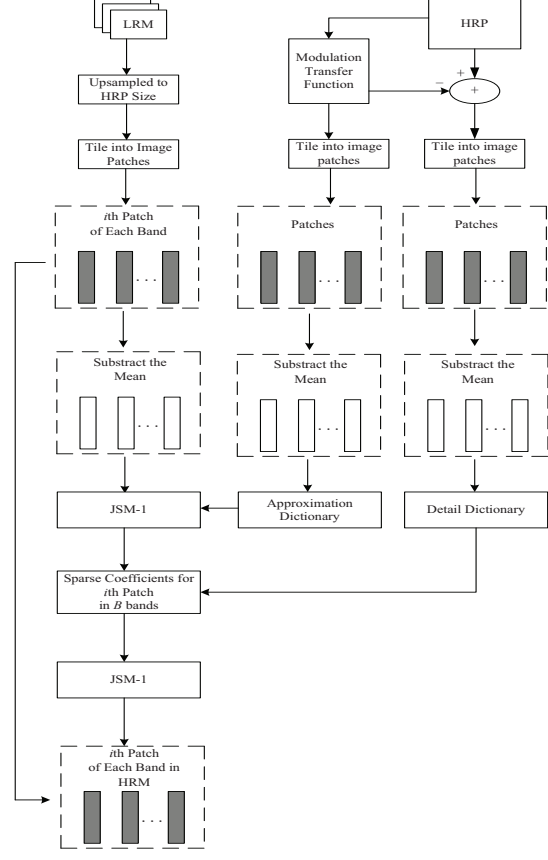
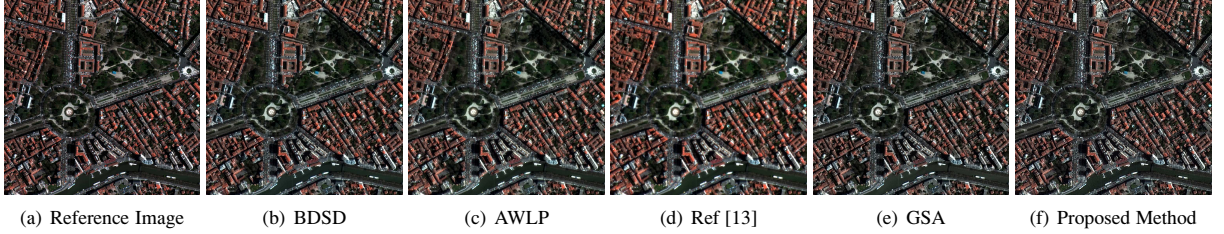


Fig. 1: Flowchart of the proposed method.

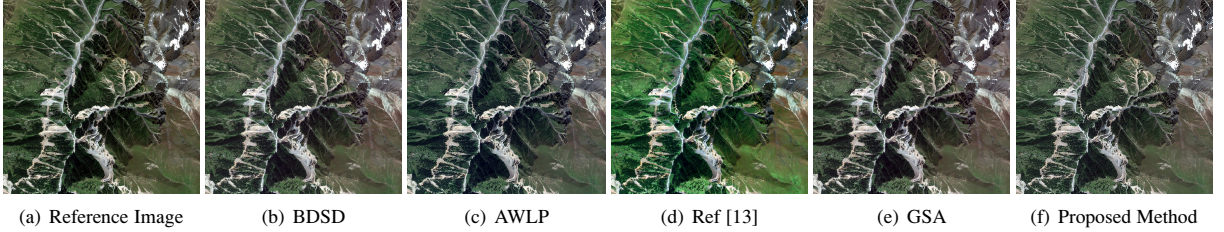
3. EXPERIMENTAL RESULTS AND DISCUSSION

For the purpose of validating the proposed method, two datasets including Pléiades data and GeoEye1 data are utilized. All the multiple spectral images from these two datasets have four spectral bands (blue, green, red and near IR). For the experimental results evaluation, the Walds synthesis protocol [16] is chosen. Based on this protocol, original LRM image is defined as a reference image. And the original LRM image and HRP image are decimated by a scale ratio which equals to the number of spectral bands. The decimated LRM and HRP images are fused to generate the HRM image which is compared with the original LRM image to assess the performance of fusion method. The fusion results are evaluated by the quaternion-based coefficient ($Q4$) [17], the Spectral Angle Mapper (SAM) [18] and the Erreur Relative Globale Adimensionnelle de Synthèse (ERGAS) [19]. A review in [1] is provided by making a critical description and exhaustive comparisons of some of the main state-of-the-art fusion methods which are utilized in the experiments to gauge the performance. The typical traditional methods chosen for



(a) Reference Image (b) BDSD (c) AWLP (d) Ref [13] (e) GSA (f) Proposed Method

Fig. 2: Fusion Results of Different Methods with Pléiades Data



(a) Reference Image (b) BDSD (c) AWLP (d) Ref [13] (e) GSA (f) Proposed Method

Fig. 3: Fusion Results of Different Methods with GeoEye1 Data

comparison include BDSD [5], AWLP [6], reference [13] and GSA [20] (improved GS). In the experiments, the patch size is set as 64×64 with overlap $r = 50\%$ and the measurement matrix is Gaussian random sampling matrix.

3.1. Experiments with Pléiades Data

Fig. 2 indicates fusion results of different methods with Pléiades data, where (a) is the reference LRM image with size 1024×1024 pixels, (b)-(e) are the fusion results of the traditional methods, and (f) displays the fusion image of the proposed method. It can be found from Fig. 2 that the fusion image of the proposed method stays more natural to the reference image especially compared with DCS-based Ref [13]. Table 1 lists the quality metrics of different fusion methods, where the best result of each metric is displayed in bold. One observes that the proposed method have the best $Q4$ and SAM performance and the second best ERGAS performance.

3.2. Experiments with GeoEye1 Data

Fusion results of different methods with GeoEye1 data are shown in Fig.3, where (a) is the reference LRM image with size 2048×2048 pixels and (b)-(f) show the fusion results of different methods. It can be seen again that spectral details in the fusion image of the proposed method is more similar to the reference image than other fusion methods. Quantitative results are listed in Table 2, where the boldest result is the best one. It is clear that the proposed method has the best performance for all the quality indexes. This is to say, the fusion image of the proposed method is better for preserving the spectral characteristics.

Table 1: Pliades Data: Results of Different Methods

	BDSD	AWLP	Ref [13]	GSA	Proposed
$Q4$	0.9650	0.9426	0.9077	0.9572	0.9725
ERGAS	2.7811	3.5219	4.7308	3.0013	2.9635
SAM	4.0749	4.3356	4.7122	4.4449	3.9445

Table 2: GeoEye1 Data: Results of Different Methods

	BDSD	AWLP	Ref [13]	GSA	Proposed
$Q4$	0.8351	0.8457	0.7960	0.8390	0.8519
ERGAS	2.9062	2.9526	4.7920	2.8538	2.7610
SAM	3.3887	3.3346	3.9178	3.2487	3.1643

4. CONCLUSION

This paper has proposed a new method to obtain high-resolution multispectral image based on DCS, where JSM-1 is applied directly to both the LRM and HRM images. For the LRM image, each LRM band is decomposed into common component and innovation component over approximation dictionary learned from the low-pass version of the HRP image and then the sparse coefficients are calculated from JSM-1 of LRM bands. For the HRM image, each HRM band is constructed by adding detail band over the detail dictionary generated from the high-pass version of the HRP image to the corresponding LRM band. The proposed method is profitable for utilizing the correlation among multispectral bands and preserving the spectral features of each band. Experimental results indicate that this proposed method is better than the traditional methods.

5. REFERENCES

- [1] G. Vivone et al., “A critical comparison among pan-sharpening algorithms,” *IEEE Transactions on Geoscience and Remote Sensing*, vol. 53, pp. 2565–2586, May 2015.
- [2] M. Ghahremani and H. Ghasseman, “A compressed-sensing-based pan-sharpening method for spectral distortion reduction,” *IEEE Transactions on Geoscience and Remote Sensing*, vol. 54, pp. 2194–2206, Apr. 2016.
- [3] W. J. Carper, T. M. Lilles, and R. W. Kiefer, “The use of intensity-hue-saturation transformations for merging spot panchromatic and multispectral image data,” *Photogrammetric Engineering and Remote Sensing*, vol. 56, pp. 459–467, April 1990.
- [4] C. A. Laben and B. V. Brower, “Process for enhancing the spatial resolution of multispectral imagery using pan-sharpening,” *Websterny Usopenfieldny Us*, 2000.
- [5] A. Garzelli, F. Nencini and L. Capobianco, “Optimal mmse pan sharpening of very high resolution multispectral images,” *IEEE Transactions on Geoscience and Remote Sensing*, vol. 46, pp. 228–236, Jan. 2008.
- [6] X. Otazu, M. Gonzalez-Audicana, O. Fors and J. Nunez, “Introduction of sensor spectral response into image fusion methods. application to wavelet-based methods,” *IEEE Transactions on Geoscience and Remote Sensing*, vol. 43, pp. 2376–2385, Oct. 2005.
- [7] Man Wang, Jie-Lin Zhang and Dai-Yong Cao, “Fusion of multispectral and panchromatic satellite images based on ihs and curvelet transformations,” in *2007 International Conference on Wavelet Analysis and Pattern Recognition*. IEEE, 2007, pp. 321–325.
- [8] V. P. Shah, N. H. Younan and R. L. King, “An efficient pan-sharpening method via a combined adaptive pca approach and contourlets,” *IEEE Transactions on Geoscience and Remote Sensing*, vol. 46, pp. 1323–1335, May 2008.
- [9] S. A. Valizadeh and H. Ghasseman, “Remote sensing image fusion using combining ihs and curvelet transform,” in *6th International Symposium on Telecommunications (IST)*. IEEE, 2012, pp. 1184–1189.
- [10] S. Li and B. Yang, “A new pan-sharpening method using a compressed sensing technique,” *IEEE Transactions on Geoscience and Remote Sensing*, vol. 49, pp. 738–746, Feb. 2011.
- [11] D. Baron et al., “Distributed compressive sensing,” pp. 2886–2889., 2009.
- [12] Q. H. Zhang, Y. L. Fu, H. F. Li and J. Zou, “Dictionary learning method for joint sparse representation-based image fusion,” *Optical Engineering*, vol. 52, May 2013.
- [13] J. Liu, X. C. Li, K. J. Zhu and K. Y. Huang, “Distributed compressed sensing based remote sensing image fusion algorithm,” *Journal of Electronics and Information Technology*, vol. 39, pp. 2374–2381, Oct. 2017.
- [14] S. G. Mallat and Zhifeng Zhang, “Matching pursuits with time-frequency dictionaries,” *IEEE Transaction on Signal Processing*, vol. 41, pp. 3397–3415, Dec. 1993.
- [15] M. Ghachili and H. Ghasseman, “Fusion of remote sensing images based on dictionary learning,” in *2017 Iranian Conference on Electrical Engineering (ICEE)*. IEEE, 2017, pp. 1895–1900.
- [16] L. Wald, T. Ranchin and M. Mangolini, “Fusion of satellite images of different spatial resolutions: Assessing the quality of resulting images,” *Photogrammetric Engineering and Remote Sensing*, vol. 63, pp. 691–699, Jun. 2009.
- [17] L. Alparone, S. Baronti, A. Garzelli and F. Nencini, “A global quality measurement of pan-sharpened multispectral imagery,” *IEEE Geoscience and Remote Sensing Letters*, vol. 1, pp. 313–317, Oct. 2004.
- [18] R. H. Yuhas, A. F. H. Goetz and J. W. Boardman, “Desrimination among semi-arid landscape endmembers using the spectral angle mapper (sam) algorithm,” in *Summaries of the Third Annual JPL Airborne Geoscience Workshop*, 1992, pp. 147–149.
- [19] L. Wald, “Data fusion. definitions and architectures - fusion of images of different spatial resolutions,” 2002.
- [20] B. Aiazzi, S. Baronti and M. Selva, “Improving component substitution pansharpening through multivariate regression of ms+pan data,” *IEEE Transactions on Geoscience and Remote Sensing*, vol. 45, pp. 3230–3239, Oct. 2007.